Optics Letters

# Photopolymerization with high-order Bessel light beams

Yoshihiko Arita,[1,2,6,†] Junhyung Lee,[3,†] Haruki Kawaguchi,[3] Reimon Matsuo,[3] Katsuhiko Miyamoto,[2,3] Kishan Dholakia,[1,3,4,5] and Takashige Omatsu[2,3,*]

[1]SUPA, School of Physics and Astronomy, University of St. Andrews, North Haugh, St. Andrews, KY16 9SS, UK
[2]Molecular Chirality Research Center, Chiba University, 1-33 Yayoi-cho, Inage-ku, Chiba-shi 263-8522, Japan
[3]Graduate School of Science and Engineering, Chiba University, 1-33 Yayoi-cho, Inage-ku, Chiba-shi 263-8522, Japan
[4]College of Optical Sciences, The University of Arizona, 1630 East University Boulevard, Tucson, Arizona 85721-0094, USA
[5]Department of Physics, College of Science, Yonsei University, Seoul 03722, South Korea
[6]e-mail: ya10@st-andrews.ac.uk
*Corresponding author: omatsu@faculty.chiba-u.jp

Received 23 April 2020; revised 5 June 2020; accepted 5 June 2020; posted 8 June 2020 (Doc. ID 396012); published 15 July 2020

**We study photopolymerization with high-order Bessel light beams with phase singularities on-axis. Self-trapping and self-focusing of propagation-invariant light beams in a photopolymer allow the fabrication of extended helical microfibers with a length scale of a centimeter, which is more than an order of magnitude larger than the propagation distance of the Bessel light beams. We show the evolution of microfibers rotating at a rate proportional to the incident optical power, while the periodicity of the helical structures remains constant, irrespective of the laser power. This suggests that optical momentum transfer plays a predominant role in the growth and rotation of such fiber structures.**



https://doi.org/10.1364/OL.396012

Photopolymerization is the light-induced process of reacting monomer molecules to form polymer chains of a three-dimensional network within light-curing resins. One of the important classes of photopolymerization is the creation of self-written waveguides (SWWs) [1]. When exposed with low average optical power, self-trapping and self-focusing of light beams or optical solitons can occur along the beam propagation axis, leading to the formation of microfiber structures [2]. SWWs can have wider implications for the design of integrated optical circuits and devices in optical sensing and communications [3,4] as well as for the rapid fabrication of high aspect ratio microstructures without beam scanning [5].

Recently we demonstrated photopolymerization with Laguerre–Gaussian (LG) beams carrying orbital angular momentum (OAM) in the self-focusing regime [6,7]. Due to the presence of a phase singularity on the beam axis, LG beams exhibit an annular intensity profile in the direction transverse to the beam propagation axis. Such beams have gained prominence due to a diverse range of applications, e.g., in optical manipulation [8–10] and materials processing [11–13]. When launched into a self-focusing photopolymer, photopolymerization creates an optical vortex-soliton with a spiral trajectory [14], which results in an associated helical microfiber with a chirality determined by the sign of $\ell$. Within the paraxial limit, our theoretical model, based on the nonlinear Schrödinger wave equation for the slowly varying electric field due to the permanent refractive index change [2], captures the main features of the experiment. These fabricated helical microfibers have the potential to provide new devices for mode generation, sorting, and optical communications, all based on OAM modes [15–17]. However, a major drawback to these applications is the limited length of these fibers (<200 μm) when created using LG modes [6]. Furthermore, the detailed mechanism of the growth of such fiber structures, specifically the role of optical forces acting on solidified polymers, remains unclear, and no quantitative conclusions have been made.

In this Letter, we investigate photopolymerization in response to high-order Bessel beams (BBs) possessing OAM at the visible wavelength of 532 nm. BBs are propagation-invariant beams, often termed "diffraction free," which can persist for distances much longer than the Rayleigh limit. To date, zeroth-order BBs have demonstrated a successful fabrication of microfiber structures without a twist [18–23]. Here we launch the first-order BBs with a propagation range of >700 μm in a photopolymer. Self-trapping and self-focusing of the BBs lead to the formation of optical vortex-solitons and associated helical microfibers with a length scale of a centimeter, which is more than one order of magnitude larger than the propagation distance of the BBs. The rotation of microfibers is observed at a rate (up to 30 Hz) proportional to the incident optical power, while the periodicity of the helical structures, i.e., helical density, remains constant, irrespective of the laser power. This suggests that optical momentum transfer plays a predominant role in the growth and rotation of such fiber structures in a photopolymer. High-order BBs offer significant advantages for the fabrication

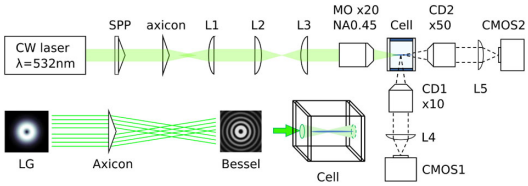


**Fig. 1.** Schematic of the experimental setup. A linearly polarized Gaussian beam is converted to a LG beam by a spiral phase plate (SPP). The vortex beam is further modulated by an axicon to generate a Bessel beam carrying OAM, which is relayed by a set of lenses (L). A far-field annular ring (the Fourier transform of the Bessel beam) is focused by a microscope objective (MO) inside a sample cell containing a resin (NOA63) to initiate photopolymerization, which is monitored by side- and axial-view cameras (CMOS1; CMOS2) through condenser lenses (CD1; CD2). The inset shows a ray diagram of LG to Bessel beam conversion through the axicon and the high-order Bessel beam focused in the sample cell.

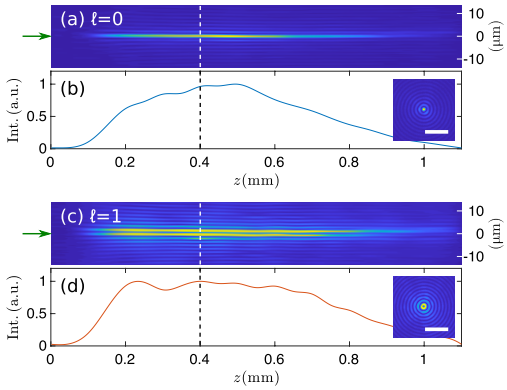


**Fig. 2.** Bessel beam profiles along the beam propagation direction ($z$ axis). (a), (c) Zeroth- and first-order beam profiles on a plane through the $z$ axis, where green arrows indicate the incident beam direction, and (b), (d) their intensity profiles. Inset panels are transverse beam profiles at $z = 0.4$ mm, where the scale bars indicate 10 μm.

of helical microfiber structures over extended ranges of $\gtrsim 1$ cm when compared to LG light beams. Helical fibers of this length would be a significant step forward towards real applications in optical communications with OAM modes [24].

To obtain a high-order BB, we illuminate a conically shaped optical element termed an axicon with a LG light beam of order $\ell$, which transforms this beam into an approximation to a high-order BB of order $\ell$ [25]. Figure 1 shows a schematic diagram of the experimental setup. A linearly polarized continuous-wave laser with a wavelength of 532 nm is converted to a LG beam of order $\ell = 1$ by a spiral phase plate (SPP) followed by the axicon (apex angle 175°). The generated high-order BB is relayed by a set of lenses (L) to a microscope objective (MO, Mitutoyo M Plan Apo, ×20, NA = 0.42, WD = 20 mm), which is used to initiate photopolymerization. A sample cell with a type-1 cover glass window (VWR, 150 μm in thickness) contains 0.8 mL of a UV curing resin (Norland, NOA63).

We first characterize the high-order BB and compare it with the zeroth-order BB. Figure 2 shows these beam intensity profiles along the beam propagation direction after the MO [see Fig. 1]. The zeroth-order BB extends over ∼600 μm (FWHM) in length with multi-ringed side lobes [Figs. 2(a) and 2(b)], while the first-order BB exhibits a dark center with a propagation range of ∼0.75 mm (FWHM) [Figs. 2(c) and 2(d)]. Inset panels show the transverse beam profiles at $z = 0.4$ mm, where the beam diameters are 0.9 μm and 2.3 μm, respectively. We note that this propagation range is more than an order of magnitude larger than the Rayleigh range of the LG beam with $\ell = 1$ using the same optical system.

When the resin is exposed with a low average optical power ($0.7\ \text{W} \le P \le 0.9\ \text{W}$), photopolymerization induces a positive refractive index change of the resin at a lag time or a critical exposure time $\tau_c$ (between the application of the laser field and the appearance of the optically induced refractive index change typically within a period of $5\text{s} \le \tau_c \le 25$ s depending on the optical power) from $n_{\text{unc}} = 1.52$ up to $n_{\text{cur}} = 1.56$ (when completely polymerized). Multi-ringed polymerization due to the outer rings of the BB can be avoided by adjusting the optical power ($P < 1.6$ W) so that only the central annulus performs polymerization. The refractive index change of the resin causes scattering of the incident beam. We use this to visualize photopolymerization in the plane of the beam axis using a side-view camera (CMOS1, Basler AG, acA1300-200um, 500 fps) perpendicular to the beam axis. Transmitted light through the resin is also recorded by an axial-view camera (CMOS2, Basler AG, 500 fps) to measure the rotation rate of the microfiber [see Fig. 1]. We note that to avoid undesired refraction effects due to the index mismatch at the glass–resin interfaces of the sample cell, the incident beam is focused inside the resin away from these boundaries to initiate polymerization.

We first investigate photopolymerization with LG beams, and compare this with the BB case. Figure 3(a) shows a side-view image of the scattered light from a short microfiber (<0.1 mm) polymerized by a LG beam with $\ell = 1$ after light exposure of 0.5 W, which yields a comparable power density with the corresponding BBs, for 1 s using the same optical setup in Fig. 1 but without the axicon and L1. We note that this observation is comparable with our previous LG beam polymerization study at the wavelength of 405 nm [6], and the fiber does not increase its length with longer light exposure (>1 s) or with different incident optical power.

In comparison, when the first-order BB with $P = 0.75$ W is focused in the resin with light exposure of 13 s, a long strand of microfiber (>1 mm limited by the field of view) is formed along the incident beam axis [Fig. 3(b)], which is the same $z$ axis coordinate in Fig. 2, beyond its propagation range ($z \gtrsim 0.75$ mm). Indeed, as shown later, the polymerized fiber structures are typically on a length scale of a centimeter. The self-trapping of the BBs in the photopolymer creates fibers much longer than the propagation invariant distance of the beam. Thus, optical vortex-solitons in high-order BBs lead to the formation of helical microfibers in the photopolymerization process.

Figure 3(c) shows combined line spectra, where each spectrum (or row of the image) represents scattered light intensities along the beam ($z$) axis, measured at a time between 11.7 s and 13.7 s (corresponding to the vertical axis) with a resolution of 2 ms. This time-lapse image of the fiber indicates that photopolymerization starts at around $t = 12\ \text{s} (= \tau_c)$, and the fiber extends in both forward and backward directions along the beam axis due to the presence of the back-scattered light guided through the fiber itself from both fiber ends [18]. Figure 3(d) shows the variation of the total scattered light intensity (blue curve) during the light exposure for 15 s, which is obtained by the sum of each row's elements in Fig. 3(c). The rapid increase

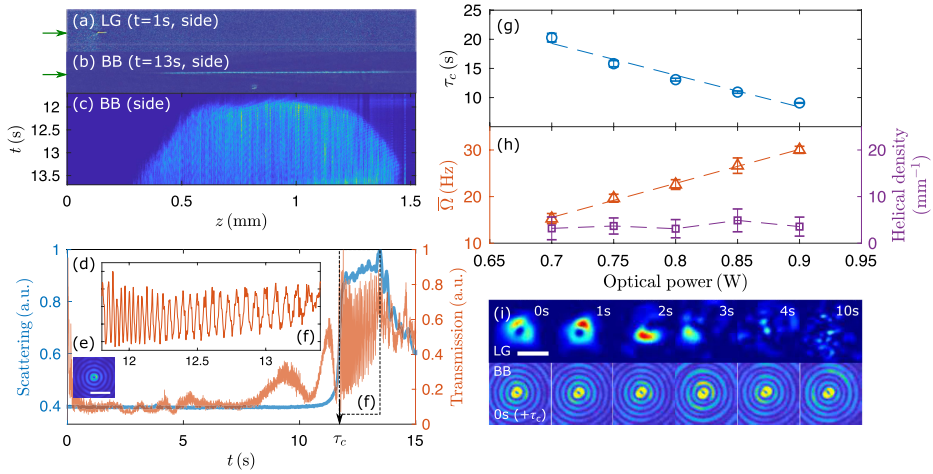


**Fig. 3.** Photopolymerization with (a) a LG beam with $\ell = 1$ and (b) first-order Bessel beam ($\ell = 1$) recorded by the side-view camera (CMOS1) showing scattered light from the fiber, where the green arrow indicates the incident beam direction. (c) Time-lapse image of scattered light along the incident beam at $11.7\ \text{s} \le t \le 13.7\ \text{s}$. (d) Total scattered light intensity (blue) and transmitted light intensity (orange) during light exposure for 15 s. (e) Transverse Bessel beam profile (recorded by CMOS2, scale bar 5 μm). (f) Expanded view of the dashed enclosed area in the period of $11.8\ \text{s} \le t \le 13.4$ s. See also Visualization 1. (g) Critical exposure time $\tau_c$ required for photopolymerization and (h) mean rotation rate $\overline{\Omega}$ and helical density of microfibers for different incident optical powers. Experimental data of $\tau_c$ and $\overline{\Omega}$ with error bars of $2\sigma$ are fitted with linear regression lines. (i) Time-lapse images of the transmitted light intensity pattern of LG ($P = 0.5$ W) and BB ($P = 0.8$ W), where $\tau_c \approx 12$ s. The scale bar indicates 5 μm and applies to all panels.

in the scattering intensity indicates the critical exposure time $\tau_c \approx 12$ s. The transmitted light intensity [orange curve in Fig. 3(d)] measured by the single pixel intensity in the phase singularity of the incident BB [Fig. 3(e)] illustrates the rotation of the microfiber [Fig. 3(f)], as previously reported in Ref. [6]. The fast intensity modulation coincides with the progression of photopolymerization, where a mean rate of rotation $\overline{\Omega} \approx 20$ Hz is measured during a period of $11.8 \le t \le 13.4$ s. Visualization 1, recorded by CMOS1 and CMOS2, shows the rapid growth of the fiber along the beam axis and its rotation around the beam axis after $\tau_c$.

Figure 3(g) shows the critical exposure time $\tau_c$ required for photopolymerization to start, at which time the scattering intensity rapidly increases [see blue curve in Fig. 3(d)] corresponding to the optically induced refractive index change. $\tau_c$ decreases proportionally with the incident optical power $P$ in the range of 0.7−0.9 W. The mean rotation rate $\overline{\Omega}$ of the microfiber, on the other hand, is proportional to $P$ with a gradient of 73.0 $\text{HzW}^{-1}$ [orange triangles in Fig. 3(h)], which is measured by the number of revolutions in the period between $\tau_c$ and $\tau_c + 1.5$ s at each optical power.

Figure 3(i) compares the transmitted light intensity pattern between the LG and BB during the laser irradiation recorded by the axial-view camera (CMOS2). The LG beam guided through the polymerized fiber loses its beam character and turns into the speckle pattern due to light scattering by the short LG fiber (<0.2 mm). When we consider the long extended BB fiber, the transmitted light stays largely unchanged, suggesting that the BB wavefront is maintained throughout the structure.

Once polymerized, microfibers are collected from the sample cell, and any uncured resin is removed by acetone. Care must be taken in order not to damage the microfibers when transferring them onto a microscope cover glass for imaging. We note that there is a risk of altering the fiber structure or the breakup of the fiber during these sample treatments. Nevertheless, we find microfibers with a length in the range of 0.5 cm−1 cm with the microscope objective (NA = 0.42) used. Figure 4(a) shows a typical example of fabricated microfibers with a length of 5.8 mm and a mean diameter of 6 μm when irradiated with the incident optical power of 0.85 W for the duration of 15 s. The helical structure of the fiber can be identified in the cross-polarized image [Fig. 4(b)], where we find 39 dark segments representing the helical features. This yields the helical density of 6.7/mm, which is within the error of $2\sigma$ at 0.85 W in Fig. 3(h). Figures 4(c) and 4(d) are expanded views of the dashed enclosed areas in Figs. 4(a) and 4(b), respectively, showing the details of the microfiber. Here we find that the pitch of the helical structure is not evenly spaced across the fiber. The original structure of the fiber may have been altered because of the vigorous acetone treatment after photopolymerization. To obviate this in future, one could for instance perform photopolymerization in a microfluidic channel, where the resin can be washed away by a steady flow of acetone to minimize deformation of the polymerized fiber. We also note that linear polarization breaks the cylindrical symmetry of the BB, which in turn affects the fabricated microfiber structures. The use of circular polarization may be preferable for improving the quality of the polymerized fiber. Nevertheless, the density of the helical features is measured (>10 samples for reliable statistics) for each collected microfiber polymerized for each optical power (0.7−0.9 W). Figure 3(h) compares the helical density (purple squares) with the mean rotation rate $\overline{\Omega}$ (orange triangles) at different optical powers, where the density remains unchanged, while $\overline{\Omega}$ is proportional to the optical power. We note that the use of high-order BBs allows to imprint many helical features (typically $\gtrsim 50$) on a long extended fiber structure ($\gtrsim 1$ cm), thus yielding reliable measurements of the helical density compared with LG beam polymerization exhibiting two to three features on a short microfiber (<200 μm).

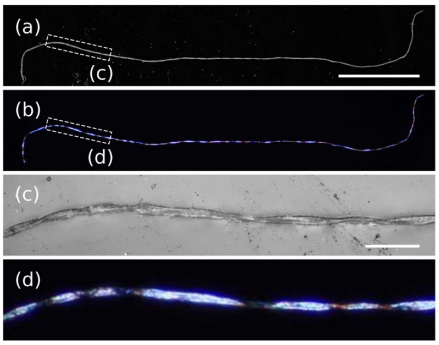


**Fig. 4.** Optical microscope images of a helical microfiber with a length of 5.8 mm. (a) Dark-field image where the scale bar indicates 1 mm. (b) Cross-polarized image where dark sections represent spiral features. (c) Bright-field image of the enclosed section in (a), where the scale bar indicates 100 μm. (d) Expanded view of the enclosed-section in (b).

Recently, in addition to our theoretical analysis [6], Nagura *et al.* have proposed a plausible model for the formation of helical fibers in photopolymerization with LG beams [26]. This model assumes that nanometric coarse-grains of polymer are first generated at the focal plane of the beam, which are subsequently launched into the vortex light field, where the Rayleigh scattering theory is applied to calculate optical forces and torques on these particles and simulate their motion. Considering submicrometer Rayleigh particles launched in a beam with the complex field amplitude of $E(r,\phi,z) = E_0(r,z)\exp(i\ell\phi)$, both the $z$ component of the gradient and scattering forces ($F_{\mathrm{grad},z}$, $F_{\mathrm{scat},z}$) and the azimuthal force ($F_{\mathrm{scat},\phi}$) scale with the field amplitude $E_0^2$ [26]. Assuming $F_{\mathrm{scat},z}/F_{\mathrm{grad},z} > 1$ so that the particles are driven by the beam along its propagation (positive $z$) direction, the period of the helix $L_\mathrm{p}$ is determined by the ratio of the net force in the $z$ direction and the azimuthal force as

$$L_\mathrm{p} = 2\pi r \frac{F_{\mathrm{scat},z} + F_{\mathrm{grad},z}}{F_{\mathrm{scat},\phi}}. \quad (1)$$

This implies that the period of a helical trajectory is independent of laser power. The coarse-grained model supports Fig. 3(h) showing that the incident power of the laser has no effect on the periodicity of the helical structures, suggesting that optical forces acting on the solidified polymers are responsible for the growth and rotation of helical microfibers in BB polymerization. Although further theoretical and experimental work is required to validate the applicability of this approach, the Rayleigh scattering model may offer an alternative route to simulate the photopolymerization process, complementing the paraxial soliton numerical study we explored in previous work [6].

In conclusion, we have demonstrated photopolymerization with first-order Bessel light beams possessing OAM with phase singularities on-axis. Self-trapping and self-focusing of the propagation invariant light beams lead to the formation of optical vortex-solitons and associated helical microfibers with a length scale of a centimeter, which is more than an order of magnitude larger than the propagation distance of the BBs. The OAM of the light imprints spiraling features across microfibers, where the rotation rate (mean rate of 20 Hz) increases with the incident optical power, while the periodicity of the helical features or the helical density remains unchanged, irrespective of laser power. This suggests that optical momentum transfer plays a predominant role in the growth and rotation of such fiber structures in a photopolymer.

Additional dataset supporting this publication can be accessed at [27].

**Funding.** Core Research for Evolutional Science and Technology (JPMJCR1903); Japan Society for the Promotion of Science (JP16H06507, JP17K19070, JP18H03884); Engineering and Physical Sciences Research Council (EP/P030017/1).

**Disclosures.** The authors declare no conflicts of interest.

[†]These authors contributed equally to this work.

## REFERENCES

1. S. Shoji, S. Kawata, A. A. Sukhorukov, and Y. S. Kivshar, Opt. Lett. **27**, 185 (2002).
2. A. S. Kewitsch and A. Yariv, Opt. Lett. **21**, 24 (1996).
3. K. B. Mogensen, J. El-Ali, A. Wolff, and J. P. Kutter, Appl. Opt. **42**, 4072 (2003).
4. A. L. Pyayt, B. Wiley, Y. Xia, A. Chen, and L. Dalton, Nat. Nanotechnol. **3**, 660 (2008).
5. U. Streppel, P. Dannberg, C. Wächter, A. Bräuer, and R. Kowarschik, Appl. Opt. **42**, 3570 (2003).
6. J. Lee, Y. Arita, S. Toyoshima, K. Miyamoto, P. Panagiotopoulos, E. M. Wright, K. Dholakia, and T. Omatsu, ACS Photon. **5**, 4156 (2018).
7. T. Omatsu, K. Miyamoto, K. Toyoda, R. Morita, Y. Arita, and K. Dholakia, Adv. Opt. Mater. **7**, 1801672 (2019).
8. Y. Arita, M. Chen, E. M. Wright, and K. Dholakia, J. Opt. Soc. Am. B **34**, C14 (2017).
9. M. Mazilu, Y. Arita, T. Vettenburg, J. M. Auñón, E. M. Wright, and K. Dholakia, Phys. Rev. A **94**, 053821 (2016).
10. M. Chen, M. Mazilu, Y. Arita, E. M. Wright, and K. Dholakia, Opt. Lett. **38**, 4919 (2013).
11. K. Toyoda, K. Miyamoto, N. Aoki, R. Morita, and T. Omatsu, Nano Lett. **12**, 3645 (2012).
12. M. Watabe, G. Juman, K. Miyamoto, and T. Omatsu, Sci. Rep. **4**, 4281 (2014).
13. F. Takahashi, S. Takizawa, H. Hidai, K. Miyamoto, R. Morita, and T. Omatsu, Phys. Status Solidi A **213**, 1063 (2016).
14. W. J. Firth and D. V. Skryabin, Phys. Rev. Lett. **79**, 2450 (1997).
15. P. Roth, G. K. Wong, M. H. Frosz, G. Ahmed, and P. St.J. Russell, Opt. Lett. **44**, 5049 (2019).
16. R. P. Sopalla, G. K. Wong, N. Y. Joly, M. H. Frosz, X. Jiang, G. Ahmed, and P. St.J. Russell, Opt. Lett. **44**, 3964 (2019).
17. P. Roth, Y. Chen, M. C. Günendi, R. Beravat, N. N. Edavalath, M. H. Frosz, G. Ahmed, G. K. Wong, and P. St.J. Russell, Optica **5**, 1315 (2018).
18. J. Ježek, T. Čižmár, V. Neděla, and P. Zemánek, Opt. Express **14**, 8506 (2006).
19. H. Cheng, C. Xia, M. Zhang, S. M. Kuebler, and X. Yu, Appl. Opt. **58**, D91 (2019).
20. F. Xin, M. Flammini, F. Di Mei, L. Falsi, D. Pierangeli, A. J. Agranat, and E. DelRe, Phys. Rev. Appl. **11**, 024011 (2019).
21. D. Pan, S. Liu, S. Ji, Z. Cai, J. Li, Y. Hou, W. Zhang, S. Fan, R. Li, Y. Hu, W. Zhu, D. Wu, and J. Chu, Opt. Lett. **45**, 897 (2020).
22. D. Pan, B. Xu, S. Liu, J. Li, Y. Hu, D. Wu, and J. Chu, Opt. Lett. **45**, 2584 (2020).
23. S. Ji, R. Li, Z. Cai, D. Pan, L. Yang, Y. Hu, J. Li, D. Wu, and J. Chu, Opt. Lett. **44**, 5073 (2019).
24. P. Wang, H. Zhao, T. Detani, Y. Tsuyuki, and H. Li, Opt. Lett. **45**, 1846 (2020).
25. J. Arlt and K. Dholakia, Opt. Commun. **177**, 297 (2000).
26. R. Nagura, T. Tsujimura, T. Tsuji, K. Doi, and S. Kawano, OSA Contin. **2**, 400 (2019).
27. https://doi.org/10.17630/faf035d4-198a-4d5c-bea1-751633f58042.